Renewable Energy Powered Membrane Technology: Energy Buffering Control to Reduce Shut-Down Events and Enhance System Resilience under Different Solar Days

Sheying Li, Achim Voigt, Yang-Hui Cai, Andrea I. Schäfer, and Bryce S. Richards*

Fluctuating and intermittent solar energy cause shut-down and reduce resilience of photovoltaic powered membrane (PV-membrane) systems. A charge controller based on pre-set voltage thresholds for supercapacitors (SC) is designed and employed on varied solar days to cope with these issues. Several parameters—number of shut-down events ($\#_{SD}$), shut-down duration (t_{SD}) and resilience factor in flux (RF_{flux})—are quantified. The controller reduces t_{SD} by 37% (partly cloudy) and 12% (very cloudy), and $\#_{SD}$ by 2 and 13 events, respectively. During the 90 min fluctuations, t_{SD} is shortened to 1–4.5 min and $\#_{SD}$ is reduced by 1–4 events for feed water salinities of ≤7.5 g L^{-1}. Increasing the PV power capacity to 600–1000 W, zero $\#_{SD}$ occurs and RF_{flux} rises from 0.3 to 0.8, indicating enhanced system resilience.

1. Introduction

1.1. Brackish Water Membrane Desalination System under Fluctuating and Intermittent Operation

Small-scale renewable energy (RE) powered membrane filtration systems are an attractive option for supplying clean drinking water in remote areas that lack both water and electricity distribution systems.[1,2] Based on the Sustainable Development Goal (SDG) report in 2022, 1.6 billion people will lack safely managed drinking water supplies—namely, fulfill the criteria for accessibility, availability, and quality,[3]—and 670 million people still having no access to electricity by 2030.[4] With the steady price declines

S. Li, A. Voigt, B. S. Richards
Institute of Microstructure Technology (IMT)
Karlsruhe Institute of Technology
Hermann-von-Helmholtz-Platz 1, 76344 Eggenstein-Leopoldshafen,
Germany
E-mail: bryce.richards@kit.edu
Y.-H. Cai, A. I. Schäfer
Institute for Advanced Membrane Technology (IAMT)
Karlsruhe Institute of Technology (KIT)
Hermann-von-Helmholtz-Platz 1, 76344 Eggenstein-Leopoldshafen,
Germany

over the last decade, photovoltaic (PV) energy has become an affordable source of clean electricity.[5]

Amongst the many available PV integrated applications, directly-coupled membrane filtration systems[6]—in which no energy storage components are present—offer the possibility to increase the system simplicity, efficiency, and robustness,[7] with several systems being successfully demonstrated in the field.[8–10] The main challenge is the intermittent and fluctuating nature of the solar[11] and wind resource that occur due to passage of heavy clouds or turbulence,[12] respectively, ranging from short (seconds to a few minutes) to long-term (tens to hundreds of hours) effects caused by weather systems.[13–15] In a photovoltaic powered membrane filtration (PV-membrane) system, changes in solar irradiance (SI) translate directly into varied output power (voltage, current) from the PV modules, which then induce fluctuations in pump performance (pressure, flow). Here, fluctuation is distinguished from intermittency in that, while the former might result in large variations in pressure and flux,[16] these are not necessarily enough for the pump to cease operation. In the latter case, intermittency results in a system shut-down (zero flux) during periods of insufficient power availability.[17,18] Naturally, the occurrence of zero flux is attributed to i) zero (or minimal) motor power due to the power intermittency from the PV source (e.g., heavy clouds passing) and ii) the low transmembrane pressure (TMP) not being able to overcome the osmotic pressure of the feed water, depending on the feed water salinity. Higher feed water concentrations result in increased osmotic pressure and, hence, higher TMP is required to produce flux and avoid system shut-downs.

Fluctuations can detrimentally affect the specific energy consumption (SEC, units: Wh L^{-1})—defined as the energy input to produce 1 L of water[1]—of the system during variable operation.[19] For example, Richards et al. reported that the SEC of the PV-membrane system under fluctuating conditions (simulated square waves of SI) exhibited ≈17% higher values than when operated under steady-state conditions.[20] When the same PV-membrane system was tested over a 60 min period on a solar day, the SEC during the fluctuating (cloudy) periods exhibited much higher peak values (by a factor of 2–5) than that during steady-state operation (cloudless periods).[21] In a wind-powered seawater desalination plant, the simulated results,

using a monthly average wind speed of 8.5 m s^{-1}, indicated that variable operation (with varied pressure and flowrate) resulted in 16% less permeate production with 8% higher permeate quality when compared with constant operation,[22] however, SEC values were not reported.

Intermittent operation could potentially increase the amount of wear-and-tear on the pump and motor during system shut-downs,[23] cause poorer membrane system performance,[24] and reduce membrane lifetime.[25] Additionally, it is recommended by the manufacturer that the reverse osmosis (RO) membranes should be operated at a constant permeate flowrate to extend the lifetime[26] Freire-Gormaly and Bilton[27] carried out week-long experiments with intermittent operation using an RO membrane system with groundwater. It was reported that the intermittent operation—a period of 8 h on, followed by a 16 h shutdown—no significant negative impacts on the membrane performance were observed after seven days of operation.[27] Ruiz-García and Nuez evaluated long-term performance of an on-grid full-scale brackish water RO desalination plant that was operating under intermittent conditions ($\approx$9 h d^{-1}) for 14 years (equivalent to 2000 d of operation).[18] Most notably, no replacement of the membrane was required during this period, although a performance decline was noted around halfway into this period. In particular, the permeate electrical conductivity (EC), that was originally $\approx$250 µS cm^{-1} then rose to >700 µS cm^{-1}, permeate production decreased by 50% and the SEC increased from 1.8 to 2.2 Wh L^{-1}.[18] These figures suggest long-term degradation of the membrane, but nothing exceptional given its lifetime. In another wind-powered membrane system operating under intermittent conditions (simulated square waves in wind power including six periods without power), it was observed that periods of shut-down—for example, of about 3 min—did not have significant impacts on the average permeate water quality as the concentration gradient reduced over time due to the salt diffused across the membrane.[28] However, short-term (0.5–1 min) system shut-downs due to power intermittencies were considered to be detrimental to performance, causing an increase in permeate EC[28] and reducing permeate production.[29] This is because the concentration gradient is highest when the power was initially switched off due to the higher initial diffusion rate.

1.2. Energy Storage Options for Membrane Systems

To overcome the fluctuations and intermittencies, energy storage devices—batteries, for example, based on lead-acid (LA) or lithium-ion (Li-ion) technologies, and supercapacitors (SCs)[30]—are often implemented to provide energy for periods of low energy availability and to buffer output for such systems.[31] The classical approach to overcome the fluctuations encountered throughout the day with PV-membrane systems is the addition of LA batteries. The advantage of this solution is the relative low cost and availability of such batteries.[32,33] However, LA batteries exhibit a limited number of charge/discharge cycles—typically in the range of 1200–1800 cycles—and a lifetime of typically 3–5 years,[33] much shorter than the >20 year lifetimes targeted from PV-membrane system.[34] Li-ion batteries have increased in popularity over recent years and have been implemented in grid-connected PV systems, exhibiting and 4000 charge/discharge cy-

cles and a lifetime of 10 years.[35] Further cost reductions by a factor of 1.2–2 to be comparable with the cost of LA batteries are required before Li-ion batteries can be expected to make a greater penetration into the off-grid PV system market.[36,37] SCs have been demonstrated to be an alternative way of realizing energy buffering for a duration of a few minutes in RE powered membrane systems, enhancing both the quality and quantity of water produced.[16,38,39] SCs can exhibit very high efficiencies (up to 98%) and long operational life expectancy of 8–10 years, but, unlike batteries, they can undergo hundreds of thousands of charging cycles and are capable of providing more instantaneous power.[16]

Moreover, due to the lack of chemical substances, absence of heavy metals and ease of utilization, SCs are considered to be an ecofriendly energy solution compared to batteries.[40] They can be operated at a wide temperature range from -40 to 70 °C without significant degradation in real practice.[41] When referring to the cost, in a wind turbine pitch control system with battery and SC, it was found that the SC (assuming a lifetime of 10 years) based control system was 2.5 times cost-effective than a battery (3–5 years of lifetime) based system when considering a 20 year lifetime of a wind turbine.[40] In another wave energy converter system that was equipped with a Li-ion battery and SC, the minimum cost obtained at an optimum depth of discharge of SC and Li-ion battery was $\approx$1.2 and 3 cents per kWh, respectively.[42] The main drawback of SCs is the high self-discharge rate (calculated value of 1.5% per day[43]) compared with a LA battery ($\approx$5% per month) or Li-ion battery (1–2% per month).[33]

1.3. System Control Strategies in Membrane Systems

For a PV-membrane system, novel control strategies ought to be introduced to operate the desalination system and manage energy distribution amongst the PV resource and energy storage units (if available). The challenge is to adapt the system operation in terms of the variations of the PV source and hence obtain a low SEC, minimize the number of shut-down events (and duration thereof) and overall increase the system robustness and resilience.[44]

Several control methodologies have been implemented and examined in the RE powered systems. In a directly-coupled PV-powered water pumping system for crop irrigation, a proportional-integral control strategy was designed to regulate the direct current (DC)-link voltage and control the status of the pump during SI fluctuations.[45] In a modeled PV-membrane filtration system, a control algorithm was proposed, based on set points of feed pressure and power distribution between the feed pump and high-pressure pump, resulting in gentle variations of power distribution.[46] A seawater membrane system in the Canary Islands was designed to adapt its energy consumption to the variable power supplied by a wind turbine and minimize the system shut-downs to maintain a constant recovery.[47] A programmable logic controller with a feedback control loop was used to regulate the rotational speed of the high-pressure pump and maintain stable pressure conditions. It achieved a target constant recovery of $\approx$14% at a relatively high SEC of 10–14 Wh L^{-1} when operating with variable power of 2–11 kW (simulated square waves at wind speed of 6–10 m s^{-1}).[47]

**ADVANCED
SCIENCE NEWS**

www.advancedsciencenews.com

**ADVANCED
SUSTAINABLE
SYSTEMS**

www.advsustainsys.com

In a directly-coupled wind powered filtration system, a controller based on model predictive control (MPC)—relied on the measured outputs from the process and future predicted system response provided by a dynamic model in order to optimize the outputs—was designed to deliver the lowest SEC and widest operation range.[44] The permeate production was increased by 2.35% for 1 h of operation (10 s of resolution wind data) at a mean wind speed of 6.5 m s^{-1} and feed salinity of 35.0 g L^{-1}.[48] Another system employed a controller with a large SC bank (250 F) as an energy buffer between the PV panels and the pump to smooth the voltage output. The control was based on voltage measurement and relays for switching the power between the PV, pump, and SC.[39] Within the feed concentration (sodium chloride, NaCl) range of 8–22 g L^{-1}, the system was able to achieve a constant permeate flow at 140 L h^{-1} and water production of 1 m^3 d^{-1}.[39] A wind-powered membrane system was designed to have feedback control based on the pre-set feed pressure to store and discharge the water in the hydraulic accumulator (300 L) via three parallel sets of solenoid valves.[49] It enabled the system to be operated continuously under low wind speeds of up to 4 m s^{-1}, compared to system operation at ≥8 m s^{-1} without control. In a PV hybrid power system with fuel cells, Li-ion batteries and SCs, an energy management system based on pre-set current values of the fuel cell was proposed to maximize the state-of-charge (SOC) of the batteries (optimize cost and lifetime cycle) and minimize the consumption of hydrogen.[50] The simulated results indicated a 5% increase in SOC and 20% less hydrogen consumption.[50] In a PV-powered seawater desalination system for crop irrigation, an energy management control based on the fuzzy cognitive maps (FCM, all concepts were fuzzified in the space [0, 1]) was designed for the system operation at variable load (pressure and feed salinity) in order to determine optimal SEC and minimal cost.[51] The control used the inputs—water tank level, PV power, and battery SOC—and a fuzzy cognitive map to decide the operating point of the desalination system. The experimental results of the system exhibited a minimal SEC of around 5 Wh L^{-1} and product EC of 500–800 μS cm^{-1} at variable operating pressure of 50–60 bar, resulting in a 39% lower cost compared with a conventional design when used for lettuce irrigation.[51] Kyriakarakos et al. conducted the simulations using the FCM variable-load energy management system (EMS) on the PV-membrane system.[52] It demonstrated a daily water production of 2.2 m^3 (assuming 17 h of daily operation) without shut-down of the plant on a sunny day, indicating a 33% increase compared to the on-off method. In a hybrid PV-RO-pressure retarded osmosis (PRO) desalination system, a soft actor-critic algorithm was developed in the EMS to maximize water production and retention, while minimizing the amount of imported power from the main grid.[53] The simulated results were compared with the previously employed particle swarm optimization algorithm in the intelligent EMS.[54] In the case of two consecutive sunny days, the SEC from the main grid achieved 24% lower (0.4 and 0.5 Wh L^{-1}, respectively) while maintaining similar retention (≈96%) and net SEC of the RO-PRO (3.1 Wh L^{-1}). In the case of ten consecutive days, it accomplished a 26% improvement compared to intelligent EMS (0.6 and 0.8 Wh L^{-1}, respectively). It improved to be an efficient algorithm without any solar power generation forecasting and is more appropriate for energy management in such systems.

1.4. Excess Power to Reduce Shut-Down Events and Increase System Resilience

Oversizing the PV power is an alternative approach to increase solar power availability and help reduce system shut-down events during periods of fluctuation and intermittency in SI, while also improving system resilience. Sufficient PV power available is important to help start the pump motor, for example, as early in the day as possible to meet wintertime loads or when coping with seasonal variations, such as rainy seasons.[55] Other advantages would be reducing the size of the energy storage units (for example, batteries) and extending the system lifetime. In particular, the prices for PV modules have been decreasing steadily and reached US$0.2 per Watt-peak in early 2022.[56]

Several operations of membrane systems equipped with excess PV power have been reported. In a two-stage membrane filtration system that was powered by 2 kW of PV, a 600 W high-pressure pump was used to create the pressure required for desalinating brackish water. The excess power was used to charge the batteries (2.4 kWh) to ensure system operation at night. The system produced 4.8 m^3 of fresh water per day (10 h) at an SEC of 1.3 Wh L^{-1} when treating 2000 mg L^{-1} water[57] with the addition of batteries. A nanofiltration (NF) pilot plant, incorporating 2.3 kW of PV panels, provided 750 W of power to the pump and to two lead-acid batteries with a capacity of 230 Ah each. The PV system exhibited a daily production of 2.4 m^3 at an SEC of 4.4 Wh L^{-1} at a feed of 3000 μS cm^{-1}.[58] It is anticipated that, by increasing the PV capacity in the system, the SEC would not change significantly as the pump will only draw as much current (power) as it required.[43] The excess power from PV panels is typically used to charge the batteries[58] or dumped,[59] while in wind-powered systems, some auxiliary loads, such as dump loads (typically electric heating),[60] may need to be implemented to absorb excess power.[61] It was suggested that the size of wind turbine (unit, W)—being 2 to 3 times higher than the desalination plant capacity (determined by electrical input power, W)—was helpful to reduce the number of system shut-downs and increase the water production.

1.5. Resilience of PV-Membrane Systems

Shut-down events are considered to be part of the disruptive events in the infrastructure system; the occurrence of such events (natural or man-made) may cause a loss of system performance, which is then followed by a recovery behavior of the system. To adequately deal with disruptions, increased attention is given worldwide to the resilience of infrastructure systems.[62] In such systems, resilience is defined as its ability to bounce back from a period of poor performance following a disruption.[62] A highly resilient system can be expressed as undergoing low-performance loss and a fast recovery postdisruptions.

For PV-membrane systems, the resilience is typically affected by: i) intermittencies in power that lead to system shut-downs; ii) fluctuations in power that reduce the ability of the system to bounce back after disruptions and result in low pressure that reduces water production and quality. Boussouga et al. analyzed the system resilience of a PV-membrane system, operated with different water types and membranes, tested during a mostly

sunny solar day, that exhibited large dips in SI due to the occasional passing of heavy clouds.[19] In that work, the permeate water quality of a tight RO membrane was demonstrated to be resilient to the change of power fluctuations, but the SEC was less resilient.[19] The aforementioned wind-powered membrane system performance in terms of permeate water quality is more resilient to power intermittency during longer shut-down periods of 120 and 180 s than that for 60 s.[28] The reason has been elaborated above; consequently, the change in permeate water quality at longer off-time (120 and 180 s) was less significant than the permeate water at 60 s. It has been revealed that the PV-membrane system typically experienced disruptions due to power variations, which predominantly depends on the key aspects—feed water quality and PV power available. Therefore, the main focus of this work is to examine the system resilience as a function of feed water qualities and PV power capacity.

1.6. Research Needs

The discussions above highlight that control strategies and sufficient power availability are beneficial for reducing the number of system shut-down events and enhancing the system resilience. In previous work, an energy buffering control system for improving resilience to short-term periodic fluctuations was implemented, using the ramp rates in PV voltage (up to 2 V s^{-1}) that were chosen to represent some of the most extreme variations reported in SI data.[43,63] To date, a study of PV-membrane system performance under real weather conditions—in particular, quantifying the number of system shut-down events (and duration thereof) and seeking to enhance the system resilience to the power fluctuations and intermittencies—has not been addressed. Therefore, investigations on how the PV-membrane system behaves with effective system control—in particular with SEC, shut-down events and resilience factor (RF)—under high-temporal-resolution (1 s) and over entire solar days are required. In this work, a charge controller and control algorithm based on pre-set voltage sensing thresholds has been designed for SC-based energy buffering in a PV-membrane system. The system resilience was further demonstrated and quantified in three factors: i) the number of shut-down events ($\#_{SD}$); ii) the shut-down duration (t_{SD}); iii) RF for the dips (passing clouds) in the SI. Note, that t_{SD} represents the period of time when zero permeate flux occurs during the operation of the PV-membrane system, while $\#_{SD}$ is counted as once per period where no permeate is produced.

In this paper, three research questions are addressed: i) How can the SCs and charge controller improve system resilience under varied full-length solar days, in particular with reducing $\#_{SD}$, t_{SD} and SEC? ii) How does feed salinity affect the ability of the SCs and charge controller to reduce $\#_{SD}$ and t_{SD}? iii) Can additional PV power available reduce system shut-downs and improve resilience via the charging mechanism of SCs and charge controller? By reducing system shut-downs and enhancing resilience, improvements to the average SEC and average RF may be achieved. Performing such research using high-resolution solar resource data is paramount in the realization of resilient systems for providing clean drinking water in the off-grid areas.

2. Experimental Section

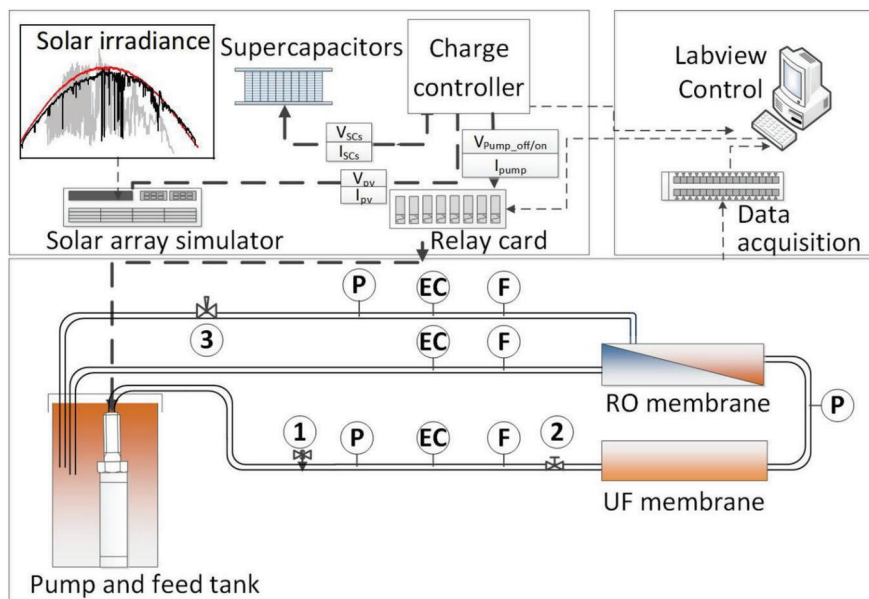### 2.1. Pilot-Scale PV-Membrane System Description

The PV-membrane system for brackish water desalination used in this study has been extensively described previously.[43] In brief, the PV-membrane system—a schematic of which is illustrated in **Figure 1**—is based on a helical rotor pump (Grundfos, SQFlex 0.6-2 N) driven by a DC motor, which pumps water first through an ultrafiltration (UF) membrane and then through a RO membrane (discussed in Section 2.2). It must be noted that this pump always seeks to extract the maximum power from the power sources due to a built-in maximum power point tracker (MPPT), which can cause a sudden drop of motor power when adding another energy source, such as SCs.[34] Consequently, in order to avoid the conflicts with the built-in MPPT of the pump, a positive temperature coefficient lamp (1500 W, Osram R7s-p15) was connected in series with the pump to increase the inner series resistance (load) as the MPPT constantly tracks the PV output and applies the load to obtain maximum power.[64] The negative side effect of adding a parasitic resistance is the induced power loss (discussed in Section 3.4, power consumption not included in the calculation of SEC). Inline sensors—pressure, flowrate, EC, temperature, current, voltage—are installed to measure all parameters under transient operation with a temporal resolution of ≈1 s. All the parameters were recorded using a data acquisition card (National Instruments, DAQ 6229) and monitored via a LabVIEW interface. Throughout all experiments, a chiller (Julabo, FC600, Germany) was utilized to achieve a constant feed water temperature of 20 ± 0.5 °C. A constant feed concentration was maintained by recycling both the permeate and concentrate streams back into the feed tank. A needle valve (③ in Figure 1, passive, AV1241) was applied to create the required back-pressure of the system, which was regulated by opening or closing the orifice with a tapered needle-shaped disc that raises and lowers with the spin of a hand wheel. An 8-channel relay card (Conrad) was used to implement the emergency shut-down in the LabVIEW to protect against the damage of the UF membrane module when the TMP_{UF} exceeds 3 bar.[65] Finally, a charge controller was proposed to distribute the energy flow either to the pump or SCs with integrated current (I_{PV}, I_{pump} and I_{SC}) and voltage (V_{PV}, V_{pump} and V_{SC}) measurements (detailed in Section 2.4). Before each experiment, a routine flush protocol with deionized water was carried out for 1 h to remove potential foulants and scalants that might be occurred during the experiments.

2.2. Feed Water Quality and Membranes

The synthetic feed water was prepared with NaCl (Sigma-Aldrich, general purpose grade, >99%) concentrations of 1.0, 2.5, 5.0, 7.5, and 10.0 g L^{-1} using deionized water (produced from BWT Moro 350, Germany, EC = 15 μS cm^{-1}) to a range of brackish water salinities (with a salinity up to 10 g L^{-1} in total dissolved solids, TDS[66]).

The UF membrane (DuPont, dizzer P4040-6.0, U.S.A., 6 m^2 surface area[65]) was employed to remove larger particles and provide physical disinfection (viruses, bacteria, turbidity), while the RO module (DuPont, BW30, U.S.A., 7.2 m^2 surface area)[67]

**ADVANCED
SCIENCE NEWS**

www.advancedsciencenews.com

**ADVANCED
SUSTAINABLE
SYSTEMS**

www.advsustainsys.com

Figure 1. Schematic of the PV-membrane system. The solid lines represent the hydraulic connections, while the long-dashed lines represent the electrical connections of the charge controller and the short-dashed lines are the input solar data and data acquisitions. ① safety valve; ② check valve; ③ needle valve for creating a back-pressure. Sensors include pressure (P), flow (F) and electrical conductivity (EC) sensor. V and I represent the measurements of voltage and current from PV, pump and SCs.

was used for monovalent salt removal (in this case, Na^+, Cl^-). The RO membrane performance parameters, such as TMP, permeate flux (J), production and SEC, were calculated using well-known relationships[68,69] after taking the measurements of the sensors in the LabVIEW. The cumulative electrical conductivity (EC_{cum}) throughout the entire solar days was calculated using Equation (1) below.[70] The cumulative TDS [g L^{-1}] was estimated from EC [mS cm^{-1}] measurements, as shown in Equation (2)[68]—assuming dissolved solids are predominantly ionic in nature[71]—by using a conversion factor ($k = 0.6$), as determined by the linear relationship between EC and NaCl concentration, as shown in Figure S1 (Supporting Information). It should be noted that NaCl was the only contributor to the TDS in this study. Furthermore, the average values of flux and SEC were calculated only during the periods where $J > 0$ L m^{-2} h^{-1}, such that the values were not distorted during the off-periods.

$$EC_{cum.} = \frac{\sum \left(Q_{Pi} \cdot t_i \cdot EC_i \right)}{\sum \left(Q_{Pi} \cdot t_i \right)} \quad (i = 1, 2, 3 \cdots) \tag{1}$$

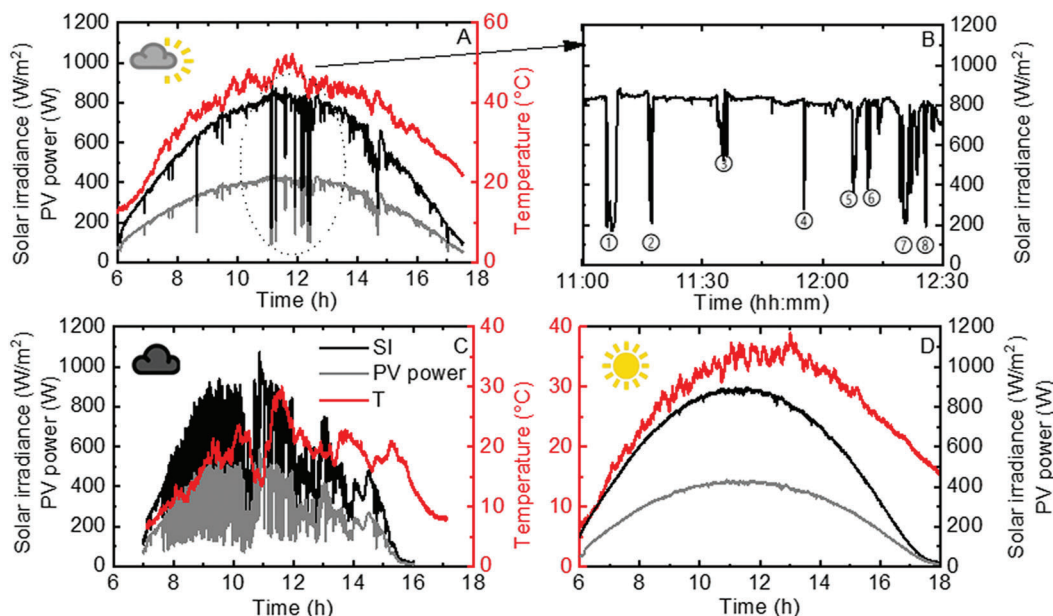$$TDS = k \cdot EC \tag{2}$$

where Q_{Pi} is the permeate flowrate [L h^{-1}], EC is the electrical conductivity of the permeate [mS cm^{-1}], t is time [h] and i represents the measured data points "number"; k is the conversion factor, 0.6.

2.3. Solar Irradiance Data and Simulated PV Output

Experiments were conducted using measured outdoor weather data to evaluate the PV-membrane system performance over three different solar days (discussed in detail below) and in two different system configurations: i) the PV power going directly to the pump, serving as the directly-coupled "reference" configuration; ii) with SC energy buffering and a charge controller. From one year (2016) of data, measured at the Karlsruhe Institute of Technology (KIT) Solar Park (1 MW capacity) in Karlsruhe, Germany, three varied full-lengthy solar days—namely sunny (5 May), partly cloudy (26 May) and very cloudy days (13 October)—were selected to represent very different levels of fluctuation in SI (1 s data resolution, 9–12 h of data). The SI [W m^{-2}] and temperature [°C] data were measured by external radiation sensors (SI-12-TC). The millisecond time values were removed and the data processed by a filtering program that replaced the invalid data from neighboring arrays. It needs to be noted that the measurements can be slightly different from real weather conditions as the dust or shadows on the PV panels might be occurred. The partly cloudy day (see **Figure 2**A) exhibited a mostly high SI, but proved challenging as eight big dips in SI were encountered from 11:00–12:30, as illustrated in Figure 2B. These dips are labeled ①-⑧ for later reference as they represent times when shut-down events are likely to occur, and subsequently they are used for the quantifications of the RF in flux during these fluctuation periods. In particular, dips (①,②,④,⑦, and ⑧) exhibiting low SI levels <300 W m^{-2} represent severe fluctuations and possess a significant challenge for the system to recover from disruptions. The SI on the very cloudy day (see Figure 2C) exhibited very rapid fluctuations due to the heavy clouds passed overhead from 7:00 to 14:00 and, subsequently, the already low SI exhibited steady reductions from 14:00 to 16:00. Instead, the sunny day exhibited uninterrupted sunshine throughout (see Figure 2D) with a typical SI in the range of 100–900 W m^{-2}. Due to the season in this latitude (beginning of May in Germany) and the temperature of

**ADVANCED
SCIENCE NEWS**

www.advancedsciencenews.com

**ADVANCED
SUSTAINABLE
SYSTEMS**

www.advsustainsys.com

Figure 2. Graphs showing the variation in solar irradiance (black curves), temperature (red curves) and the available PV power (light grey curves, rated PV capacity of 500 W) as a function of time: A) on this partly cloudy day at the KIT Solar Park (26 May 2016); B) eight large fluctuations from 11:00 to 12:30 during the middle of the day, with dips labeled from ① to ⑧ for later reference; C) very cloudy day (13 October 2016) and D) sunny day (5 May 2016).

PV modules exceeding 25 °C (see the red curve in Figure 2D), the SI does not reach 1000 W m⁻², and hence the output PV availability was even lower than that with the other two solar days. Note that the testing durations on the sunny and partly cloudy days are significantly longer as May is closer to the summer equinox (21 June).

A solar array simulator (SAS, Chroma, model 62000H) was supplied with the measured SI and temperature data from selected solar days to recreate the measured outdoor conditions. Note that the SAS simulated the PV output under real weather conditions and enabled repeatable experimental results in the laboratory environment. The available PV power (light grey curves in Figure 2) on these varied full-lengthy solar days is calculated based on the built-in Sandia model in the SAS, as shown in Equation (3):[72]

$$P = P_{REF} \cdot \frac{SI_{rr}}{SI_{rrREF}} \cdot \left[1 + \frac{\beta}{100} \cdot \left(T - T_{REF} \right) \right] \quad (3)$$
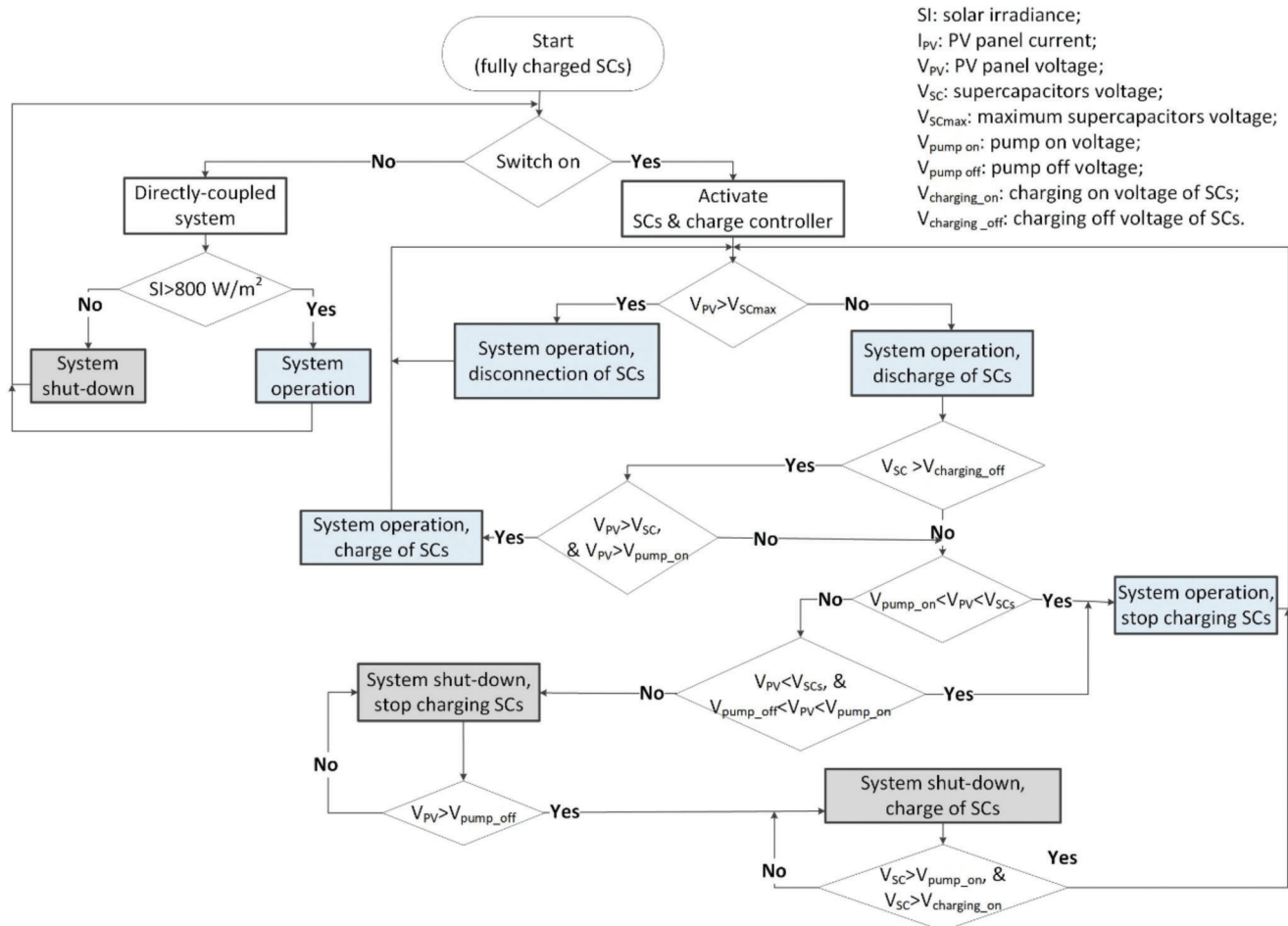
where P is the PV power [W], SI_{rr} is the solar irradiance [W m⁻²], β is the temperature coefficient of a silicon PV module [-0.41%/°C], T is the cell temperature [°C], T_{REF} is the reference array temperature (50 °C) and SI_{rrREF} is the reference irradiance (1000 W m⁻²).

For the experiments conducted in Sections 3.1–3.3, the SAS was used to simulate the output of an array of five 100 W silicon PV modules (Sunmodule, SW100 poly RGP, USA[73]) that, at the maximum power point (MPP), generate $V_{mpp} = 37.6$ V and $I_{mpp} = 2.7$ A for each PV module. With five modules connected in series, a total maximum power of 500 W can be provided at a nominal V_{mpp} of 188 V. For the final experiments (Section 3.4), the PV power capacity was varied (300, 400, 600, 800, and 1000 W) by

adjusting the photocurrent (I_{mpp} = 1.6, 2.1, 3.2, 4.3, and 5.3 A), while maintaining the same PV voltage (V_{mpp} = 188 V).

2.4. Supercapacitor Buffering and Charge Controller

For the experiments conducted with SCs in this paper, twelve modular SCs (Maxwell Boostcap, 15 V_{DC}, 58 F) were connected in series to obtain a maximum voltage of 180 V and capacitance of 4.8 F, which allows a maximum energy storage capacity of ≈21 Wh to bridge the power gap up to 8.4 min with a pump power consumption of ≈400 W (assuming PV power available from the sun). To match with the MPP voltage (V_{mpp}) of PV, twelve modular SCs were selected that defined the maximum charge voltage (180 V), hence the size of SCs based on the rated modular voltage (15 V_{DC}). A charge controller based on pre-set voltage thresholds was designed to distribute the energy between the PV resource and SCs. The operation of the controller is depicted in the flow chart (**Figure 3**), with voltage control (see conditions in diamonds) being used to trigger different events (as indicated in the rectangles). It needs to be noted that this flow chart was a simple state machine that represented slow processes. As no time critical control loop was integrated, the response times were primarily determined by reaching the voltage thresholds levels and hysteresis was implemented to prevent oscillations around switching levels. As shown on the left side of Figure 3, the SCs are activated by the charge controller via internal switch and timer at SI > 800 W m⁻², which occurred at the timeframe from 9:00 to 13:00 over the three varied full-lengthy solar days. This high SI guarantees higher power to be generated for the system operation as well as for charging the SCs. Without the timer, the repeated start-ups and shut-downs of the system will occur during the low

SI: solar irradiance;
I_{PV}: PV panel current;
V_{PV}: PV panel voltage;
V_{SC}: supercapacitors voltage;
V_{SCmax}: maximum supercapacitors voltage;
V_{pump_on}: pump on voltage;
V_{pump_off}: pump off voltage;
$V_{charging\_on}$: charging on voltage of SCs;
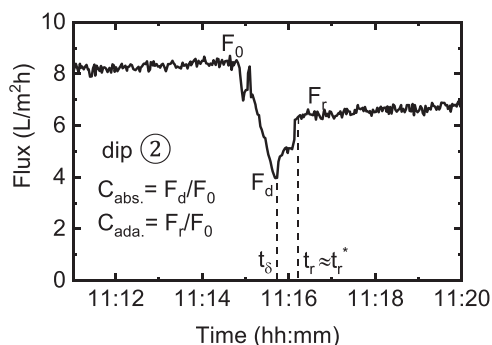$V_{charging\_off}$: charging off voltage of SCs.

Figure 3. Flow chart of the PV-membrane system operation, demonstrating the different states between pump and SCs at varied voltage conditions. Note the light blue represents the system operation, while the grey indicates system shut-down.

available PV power periods, namely early in the morning and late in the afternoon, thus room for optimization in the controller remains (discussed in Section 3.4). An overview and full electrical schematic have been described in detail in previous work.[43]

Specifically, four voltage set points were established—a lower threshold voltage to turn off the pump (V_{pump_off}), a higher threshold to turn on the pump (V_{pump_on}) and two related thresholds for determining the charging and discharging behavior of the SCs ($V_{charging\_off}$ and $V_{charging\_on}$). The voltage of the SCs (V_{sc}), pump (V_{pump}) and the PV panels (V_{PV}) is monitored to determine the status of both the pump (off or on) and the SCs (charging or discharging). The charging off/on thresholds of the SCs are selected to control the depths of charging and discharging of SCs. This approach avoids the deep discharging of the SCs at the first few fluctuations (the pump would extract less current), such that the pump can be operated continuously as much as possible when encountering several high fluctuations, thus reducing $\#_{SD}$ and t_{SD}. The decision about which operating state to be in is primarily controlled by V_{pump_off} and V_{pump_on}. Increasing the V_{pump_on} threshold value enables the pump to in the on state for a longer period due to less current being required to maintain the maximum power (built-in MPPT). While increasing the V_{pump_off} value

allows V_{PV} to charge the SCs at a higher charging rate, the disadvantage would be that the fast voltage drop from PV sources can cause unanticipated system shut-downs. A lower $V_{charging\_off}$ value effectively reduces the SOC of the SCs, which is directly proportional to the square voltage of V_{SCs}. To enable the pump to operate over a wide range of pressures, V_{pump_on} was chosen based on the set-point operation of the PV-membrane system at 10 bar (set-point operation detailed in Section 1 of the SI) and the maximum current (2.7 A) that can be supplied by the PV panels at a rated PV capacity of 500 W. The V_{pump_off} threshold was chosen based on the minimum hydraulic pressure required to overcome the osmotic pressure at a feed salinity of 5.0 g L^{-1} NaCl ($\approx$4 bar), the charging off/on voltages were selected accordingly to enable a large range of SOC. For these reasons, the four pre-set voltage thresholds were set as follows: $V_{pump\_off} = 60$ V, $V_{pump\_on} = 120$ V, $V_{charging\_off} = 80$ V, and $V_{charging\_on} = 140$ V. This corresponds to a SOC in the SCs ranging from 20% to 100%. For the current measurements, a positive current value represents the system sourcing current via either the generated photocurrent from the PV modules (I_{PV}) or the discharging current of SCs (I_{sc}), while a negative value represents the required current for powering of the pump (I_{pump}) or the charging current for the SCs (I_{sc}).

**ADVANCED
SCIENCE NEWS**

www.advancedsciencenews.com

**ADVANCED
SUSTAINABLE
SYSTEMS**

www.advsustainsys.com

Figure 4. Graphical representation of the parameters that define the concept of resilience factor of flux. The data represents dip ② of the SI fluctuations in the partly cloudy day (see Figure 2B). All parameters are defined in the main text.

2.5. Parameters of System Resilience

For the evaluations of the system resilience over the entire solar days, the key parameters $\#_{SD}$ and t_{SD} (defined in Section 1.6) along with system performance (namely motor power, TMP, flux, cumulative TDS, production and SEC), which are affected by the fluctuations in SI, are used throughout. To quantify the resilience of the PV-membrane system, the method proposed by Juan-Garcia et al.[74] was used to determine the RF. In the present work, the performance parameters were adapted to determine the RF of flux (RF_{flux}) by using Equation (4).[74] For clarification, the critical terms are demonstrated in **Figure 4** for one fluctuation in SI (dip ②). It is noted that the RF analysis is applicable for the dips in SI on the partly cloudy day (labeled ①-⑧ in Figure 2B), but cannot be applied to a solar day characterized by constantly varying weather conditions, such as the very cloudy day (Figure 2C) as a minimum time period of a few minutes is required to maintain a relative stable state.

$$RF = S_P \cdot \left(\frac{F_d}{F_0} \right) \cdot \left(\frac{F_r}{F_0} \right) \tag{4}$$

where S_p is the speed recovery factor of the system performance, F_r is the new stable performance after recovery, F_d is the performance immediately post-disruption and F_0 is the original stable system performance. The term $\frac{F_d}{F_0}$ expresses the absorptive capacity ($C_{abs.}$), which is the ability to maintain the original system performance level immediately after a disruption. The adaptive capacity ($C_{ada.}$), given by $\frac{F_r}{F_0}$, is the ability to maintain the proportion of original system performance at a new stable level after recovery. The analysis for the RF here is different from the calculations in the work of Boussouga et al.,[19] where the system performance always recovered to the initial level (such that $F_r = F_0$). The speed recovery factor represents the elapsed duration for the performance recovery after disruption, as expressed in Equation (5):[74]

$$S_P = \frac{t_\delta}{t_r^*} \cdot \exp\left[-a \left(t_r - t_r^* \right) \right] \text{ for } t_r \geq t_r^* \tag{5}$$

where t_δ is the slack time [s]—defined as the maximum amount of time after disruptions before recovery, t_r^* represents the time to

fully recover back to the initial performance again, t_r is the time to a new equilibrium state and a is the parameter controlling decay factor in resilience attributable to time to new equilibrium (see Figure 4). Here, $S_P = 1$, as $t_r = t_r^*$ and the ratio $\frac{t_\delta}{t_r^*}$ was close to unity. It is noted that the calculation of system performance is based on short timescales (a few seconds or minutes), and a few minutes are required to achieve a new stable state. Therefore, performance values associated with epochs that occur towards the end of a disruption are chosen as they are more heavily weighted than those that occur earlier in the disruption.[75]

In summary, the parameters $\#_{SD}$ and t_{SD}, and several indicators of system performance (discussed above), were used to quantify system resilience over the entire solar days in Sections 3.1 and 3.2. For the eight dips in the SI due to passing clouds (Figure 2B), the RF_{flux} was determined as a function of feed water salinity and PV power capacity and the averaged RF values plotted in Sections 3.3 and 3.4. It should be noted that the RF values approaching unity exhibit increased resilience. Data screening was carried out for the permeate flowrate given the 5 L h^{-1} lower limit of the flow sensor.
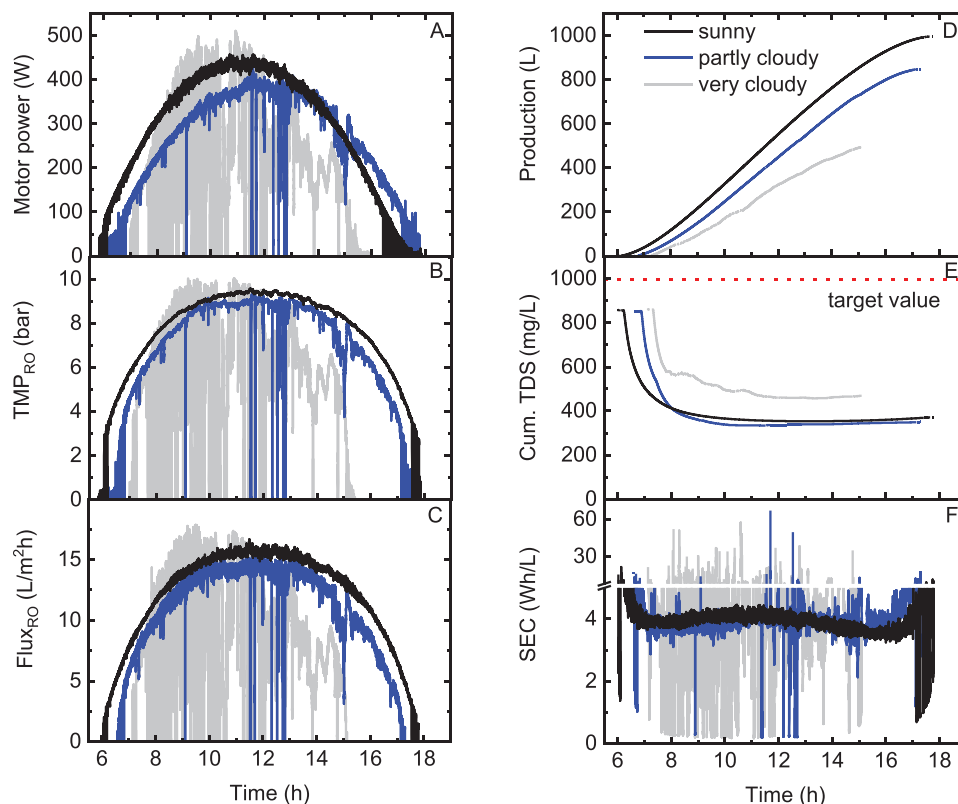
2.6. Experimental Design

The set-point operating strategy was used throughout the experiments,[29] which was achieved by regulating the back-pressure valve (③ in Figure 1) on the concentrate stream to obtain a TMP of 10 bar at feed flowrate of 420 L h^{-1} under constant power operation (detailed in Section S1 of the Supporting Information). This experimental protocol was stringently followed to check the repeatability of the data in the PV-membrane system. The experiments were undertaken using 1 s resolution of SI data and performed with the following configurations:

i) Directly-coupled PV-membrane system during the varied full-lengthy solar days—to determine the impact of varied fluctuations in SI on the resilience of PV-membrane system, using 5.0 g L^{-1} NaCl at rated PV capacity of 500 W;
ii) With SCs and charge controller during the varied full-lengthy solar days—to compare the system performance when adding the SCs and charge controller with results above (5.0 g L^{-1} NaCl, rated PV capacity of 500 W);
iii) With different feed salinities during highly variable 90 min SI fluctuations of the partly cloudy day – to examine the impacts of feed salinity on the ability of the charge controller and SCs to reduce system shut-downs and improve the system resilience (1.0, 2.5, 5.0, 7.5 and 10.0 g L^{-1} NaCl, rated PV capacity of 500 W);
iv) With varied PV power capacity during highly variable 90 min SI fluctuations of the partly cloudy day at feed salinity of 5.0 g L^{-1} NaCl—to investigate the impacts of PV capacity (300, 400, 600, 800, and 1000 W) on reducing system shut-downs and improve resilience with SCs buffering and charge controller. One additional set of experiments was repeated based on the system operating strategy to ensure repeatable results.

To check the variations of the experimental results and confirm the findings, one per experiment (specified above) was carried out by the same individual and instrument under the same operating

**ADVANCED
SCIENCE NEWS**

www.advancedsciencenews.com

**ADVANCED
SUSTAINABLE
SYSTEMS**

www.advsustainsys.com

Figure 5. Experiments conducted using the PV-membrane system under three different solar days (5.0 g L^{-1} NaCl at rated PV capacity of 500 W): A) motor power, B) TMP_{RO}, C) $flux_{RO}$, D) production, E) cumulative TDS and F) SEC. The target value—indicated by the dotted red line in (E)—of 1000 mg L^{-1} NaCl value was taken from the World Health Organization (WHO), noting that the drinking water becomes unpalatable at higher values.[76]

protocols over a short amount of time, as shown in Section S1 of the Supporting Information. All the experiments that were performed with SCs and the charge controller used the same pre-set voltage thresholds (as discussed in Section 2.3) settings for comparison.

3. Results and Discussion

3.1. Directly-Coupled System Resilience with Different Solar Days

To demonstrate the impacts of varied solar days—from sunny, partly cloudy to very cloudy—on the resilience of the directly-coupled PV-membrane system, its performance at a feed salinity of 5.0 g L^{-1} at a rated PV capacity of 500 W was investigated, as shown in **Figure 5**. These results serve as the reference to enable the comparison when SCs and charge controller are added.

During both the partly cloudy and very cloudy days, system shut-down events occurred when SI < 300 W m^{-2}, which resulted in the pump motor power (Figure 5A) dropping to 0 W several times. This sudden drop in power was also mirrored in both the TMP_{RO} (Figure 5B) and the clean water (permeate) flux (Figure 5C). The production on the sunny day (black curve in Figure 5D) exhibited the highest value of ≈1000 L, which is ≈150 L more than that on the partly cloudy day and 50% higher than the production on the very cloudy day. These results highlight the significance of having the high average SI levels (580, 545 and 430 W m^{-2} on the sunny, partly cloudy and very cloudy days, re-

spectively), and hence an adequate amount of PV power available (light grey curves in Figure 2A,C,D) over the entire solar days to produce sufficient permeate. Referring to Figure 5E, from 6:00 to 7:50 (on all days), the cumulative TDS decreased from the initially high value produced when the system was switched on. After the SI rose above 500 W m^{-2} at around 8:00, it decreased gradually until 14:00, before rising again at the end of the day, as the decrease of the SI led to small permeate volume with low quality produced. It is observed that on the very cloudy day, the gradually decreasing EC values (grey curve in Figure 5E) from 8:00 to 11:00 occurred during rapid fluctuation, indicating that system functionality has not fully recovered to its original level.[62] The SEC on the very cloudy day (grey curve in Figure 5F) exhibited the most rapid fluctuations among the varied full-lengthy solar days (average SEC of 4.6, 3.8, and 4.0 Wh L^{-1} on very cloudy, partly cloudy, and sunny day, respectively, see Table S1, Supporting Information). It indicates the impacts of flux variations caused by fluctuations of power input due to the rapid changes of SI. This is in agreement with previous observations,[20] as discussed for the cumulative water production over the entire solar days.

In order to quantify the system resilience on the three varied full-lengthy solar days of the directly-coupled system (variations in system performance discussed above, methods detailed in Section 2.5), the $\#_{SD}$ and t_{SD} (zero flux as defined in Section 1.4) are summarized in **Table 1**. No shut-down events were observed due to the good weather conditions on the sunny day. On the partly cloudy day, the PV-membrane system exhibited eight

2300031 (9 of 16)

Table 1. Directly-coupled PV-membrane system shut-down events under the entire three varied full-length solar days. Note, the system shut-downs overnight are not considered.

Solar day	$\#_{SD}$ [−]	t_{SD} [min]
Sunny	0	0
Partly cloudy	8	5.4
Very cloudy	85	119

shut-down events with a total down-time of 5.4 min, while on the very cloudy day, both the $\#_{SD}$ and t_{SD} increased dramatically to 85 and 119 min, respectively.

In summary, the directly-coupled PV-membrane system resilience over the three varied full-lengthy solar days is presented in terms of i) shut-down events quantified with adequate adaptive capacity, implying the potential for including the short-term (in the order of a few minutes) energy buffering (such as SCs) to enhance the system resilience; ii) flux to recover after fluctuations that affect permeate production; iii) permeate quality that complies with the targeted value due to the use of tight RO membrane (BW30) and iv) average SEC values in the range of 3.8–4.6 Wh L^{-1} that enable operations during the fluctuations, which exhibit varied SI levels from sunny to very cloudy days. In the next section, the shut-downs events and resilience are evaluated by adding the SCs and charge controller to the PV-membrane system.

3.2. Cumulative and Average System Performance with SCs and Charge Controller

The aim of this section is to examine the potential of the SCs and charge controller to enhance the system resilience under three entire solar days, in particular with reducing $\#_{SD}$ and t_{SD}, as well as improving SEC. Experiments were conducted (see detailed
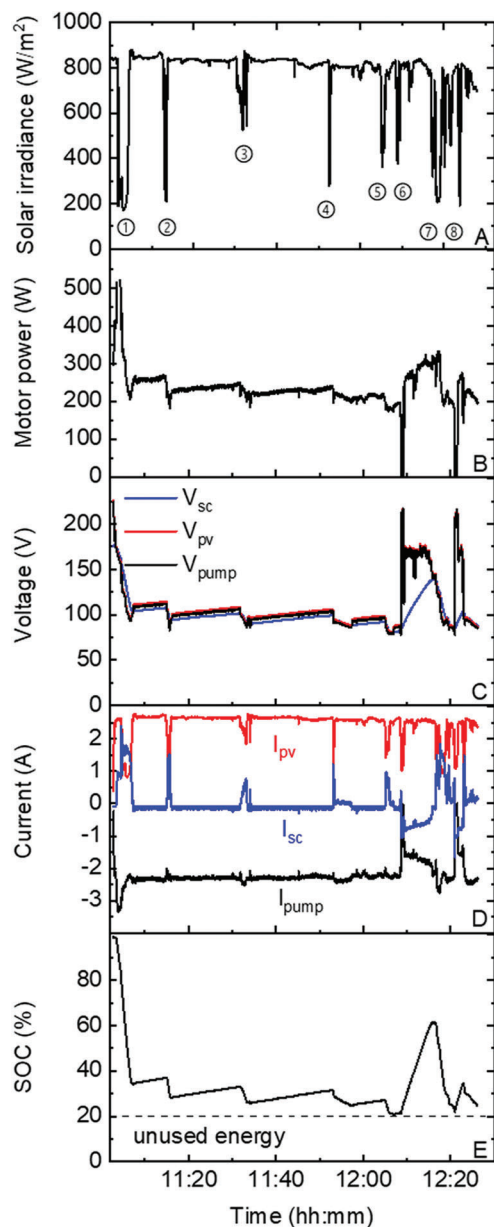
graphs provided in Figures S2–S4, Supporting Information) and then compared with the directly-coupled reference case described above. These results are plotted in **Figure 6** for further comparison.

When incorporating the SCs and charge controller, the $\#_{SD}$ was reduced by 2–13 events (Figure 6A), while the t_{SD} (Figure 6B) was reduced by 37% (partly cloudy) and 12% (very cloudy day). This indicated the improved adaptive capacity to fluctuations by including SCs and charge controller for short-term (in the order of a few minutes) energy buffering to reduce the system shut-down events. The use of SCs and charge controller made little difference to the production on the three varied full-lengthy solar days (Figure 6C), which is likely due to i) the limited capacity of the SCs not being able to buffer long periods of low SI and ii) the addition of energy storage components will reduce the system efficiency slightly, most notably via a small decline in production occurred on the sunny day. The increased capacity of SCs would provide power for longer periods of intermittency due to the inherent characteristics, which exhibit an excellent source of power, but a poor source of energy, even at a higher capacity.[77] While the smallest SCs bank was adequate for buffering the whole range of short-term fluctuations and intermittency over the system operating range, the added cost and inefficiencies to the system need to be compensated with the benefits of introducing high-capacity SCs, which also depend on the particular system and the solar resource. The average SEC is reduced by 22% (very cloudy) and 8% (sunny day) with the use of SCs and charge controller, whereas the values on the partly cloudy day remain unchanged (Figure 6D). The decrease of SEC on the very cloudy and sunny days suggests that the overall reduction of energy consumption (Wh) outweighs the impacts of the limited increase of water production [L].

In summary, the changes of pump power consumption resulted in the variations of flux (determined the $\#_{SD}$ and t_{SD}) that is mainly affected during the cloudy hours. To understand the
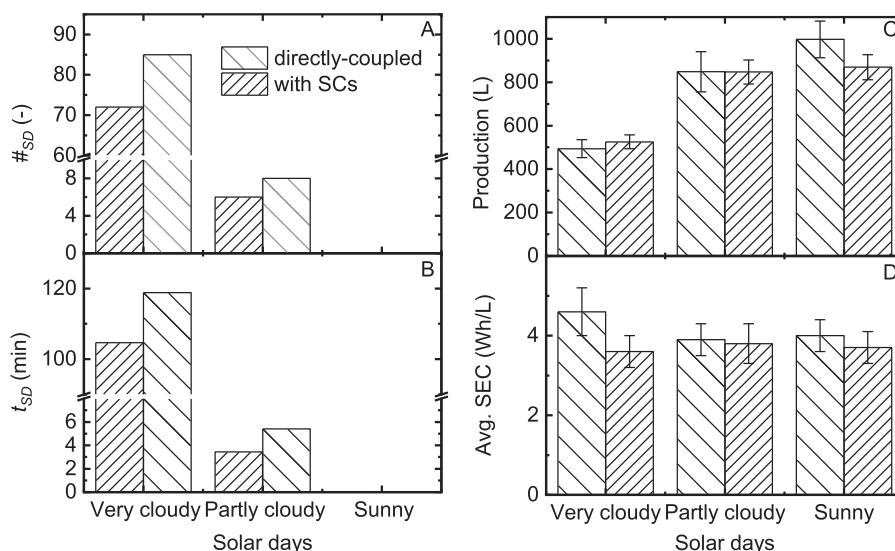
Figure 6. Bar plots of the PV-membrane system performance with/without SCs and charge controller over very cloudy, partly cloudy and sunny day at feed salinity of 5.0 g L^{-1} and rated PV capacity of 500 W, illustrating A) $\#_{SD}$, B) t_{SD}, C) production and (D) average SEC. The error bars are calculated in terms of error propagations in Section S6 of the Supporting Information. Note error bars in A and B are not needed as they represent the occurrence of definite events in certain time periods.

**ADVANCED
SCIENCE NEWS**

www.advancedsciencenews.com

**ADVANCED
SUSTAINABLE
SYSTEMS**

www.advsustainsys.com

Figure 7. PV-membrane system electrical performance in the middle of the partly cloudy day (11:00–12:30) with SCs and charge controller at rated PV capacity of 500 W and 5.0 g L^{-1} NaCl feed water salinity. A) solar irradiance, B) motor power, C) system voltages (V_{pump}, V_{SCs} and V_{PV}), D) system currents (I_{pump}, I_{SCs}, and I_{PV}) and (E) SOC.

power distribution among the PV, pump and SCs with charge controller when undergoing severe fluctuations, hence laying the foundation for quantifying the RF of flux in the 90 min time window for later investigations (Sections 3.3 and 3.4). **Figure 7** illustrates the electrical characteristics of the system performance with a duration of ≈90 min (see Figure 7A). This experiment was started at around 11:00 when SI = 800 W m^{-2} and with fully charged SCs (V_{SCs} = 177 V).

When the SI started to drop at dip ① from 850 to 200 W m^{-2} (Figure 7A), the motor power rose to ≈500 W (Figure 7B) due
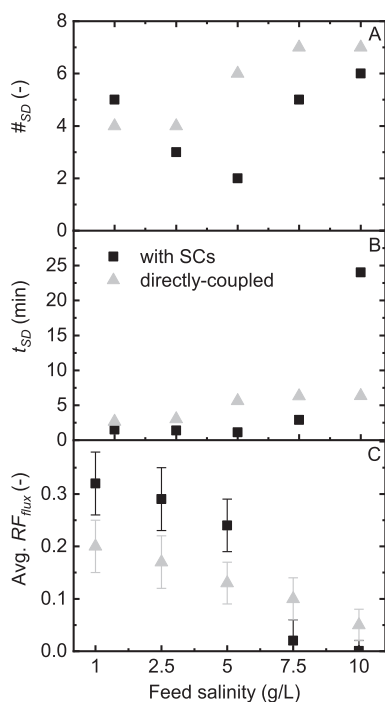
to the prompt discharge of SCs, then steadily decreased until it reached the $V_{charging\_off}$. Subsequently, the SI returned back to the high level at around 870 W m^{-2}, the V_{PV} and V_{pump} (Figure 7C) started to rise until it reached V_{pump_on} (120 V) and remained stable at this stage until the next periods of fluctuations (e.g., dip ②) were encountered. This charging/discharging behavior can be clearly observed by examining the voltages and currents from other fluctuations in the system (Figure 7C,D), as well as the SOC of the SCs (Figure 7E). The pump runs continuously during dips ①–⑤ with motor power above 200 W. It can be seen from Figure 7D that the SCs discharged to the pump promptly (added I_{sc} to I_{pump} at small I_{PV} at low SI). The small I_{sc} value (flat blue curve in Figure 7D) indicated that the I_{PV} was solely supplied to the pump when the SI returns back to high levels. This corresponds to around 10 W (error calculated to be 3.3%, see Section S6, Supporting Information) of power consumption (blue curves in Figure 7C), which contributes ≈2% of power loss. Two shutdown events are observed at dips ⑥ and ⑧ (motor power dropping to 0 W, see Figure 7B) when reaching the lower limit of the preset charge-off voltage (80 V as stated in Section 2.3) and, consequently, the I_{PV} (≈1 A) can only be used to charge the SCs (blue curve rising in Figure 7C). As indicated in Figure 7E, 20% of the energy stored in the SCs remains unused to avoid the power oscillations of the pump due to the charging requirement of the SCs at this rated PV capacity of 500 W. The maximum power loss due to the lamp is estimated to be ≈170 W (330 W power consumption at the set-point of 10 bar without lamp included[63]).

The power distribution among the PV, pump, and SCs with the charge controller during the 90 min periods has been discussed in detail above, the charge controller enabled the SCs to bridge the power gaps in an order of a few minutes during the occurrence of severe fluctuations. For the next section, the system shut-downs and resilience factor of flux during this timeframe as a function of feed salinity were examined.

3.3. Impact of Feed Salinity on System Resilience with/without SCs Buffering Control

To evaluate the impact of feed salinity on the ability of the SCs and charge controller to reduce $\#_{SD}$ and t_{SD}, as well as enhance system resilience, experiments were carried out using different feed water salinities (1.0, 2.5, 5.0, 7.5, 10.0 g L^{-1} NaCl) at the same rated PV capacity of 500 W, as displayed in **Figure 8**. The detailed system performance with/without SCs and charge controller at varied feed salinity are provided in Figures S5–S9 (Supporting Information).

For the directly-coupled system configuration, the $\#_{SD}$ and t_{SD} (see grey triangles in Figure 8A,B) indicate a rising trend when increasing the feed salinity from 2.5 to 7.5 g L^{-1}, whereas the $\#_{SD}$ and t_{SD} values remain the same at feed salinities of 1 and 2.5 g L^{-1} as well as 7.5 and 10.0 g L^{-1}, respectively. The low system resilience can be reflected from the averaged RF_{flux} < 0.2 (Figure 8C) at feed salinity of 7.5 and 10.0 g L^{-1} during this 90 min period. This occurs as the flux is reduced to 0 L m^{-2} h^{-1} at high feed salinity due to high osmotic pressure (6.3, 8.2 bar for 7.5 and 10.0 g L^{-1} NaCl, respectively), which poses a significant challenge for the system operation. Overall, increasing feed salinity increased system shut-down events and reduced system

**ADVANCED
SCIENCE NEWS**

www.advancedsciencenews.com

**ADVANCED
SUSTAINABLE
SYSTEMS**

www.advsustainsys.com

Figure 8. Impact of feed salinity on the system resilience with/without SCs buffering control during the highly variable 90 min period with large SI fluctuations in the middle of the partly cloudy day (rated PV capacity of 500 W): A) $\#_{SD}$, B) t_{SD}, C) average RF_{flux}. Note that the averaged RF_{flux} are taken from the values at each dip from ① to ⑧ as shown in Figure 2B. The error bars were estimated by using error propagation method (see Section S6, Supporting Information).

resilience, because higher driving force is required to overcome the increased osmotic pressure of the feed water at high salinity.

Once adding the SCs and charge controller, the $\#_{SD}$ is reduced by 1-4 events at feed salinities ≥ 2.5 g L^{-1}. In contrast, the $\#_{SD}$ is increased by 1 event at 1.0 g L^{-1} (black square in Figure 8A, one set of repeated results is provided in Figure S6 of the Supporting Information). This occurs as the SCs are discharging excessively at dip ① and, consequently, the I_{PV} is required to charge the SCs once the V_{PV} drops < 140 V (pre-set charging on voltage), causing one more shut-down at dip ⑤ (see Figure S5, Supporting Information). The t_{SD} is constrained to a range between 1 and 4.5 min at feed salinities of ≤ 7.5 g L^{-1}, whereas the t_{SD} duration increased dramatically at 10.0 g L^{-1} (with $\#_{SD}$ reduced once at dip ①). This can be explained by the fact that the high salinity at 10.0 g L^{-1} resulted in low flux compared to lower feed salinities. Meanwhile, system shut-down duration was prolonged due to the requirement for charging the SCs and the pump can only be restarted once V_{PV} reaches the pump on voltage value (120 V). Referring to Figure 8C, the RF_{flux} values close to 0.3 at feed salinity ≤ 5.0 g L^{-1} reflect the system in terms of flux is more resilient to power fluctuations. It was observed that the RF values were still far from ideal (unity), due to limitations in the energy storage capacity of SCs and PV power as discussed in Section 3.2. Instead, it decreased when treating high salinity water (7.5 and 10.0 g L^{-1}), which indicated the flux is less resilient to power fluctuations after energy buffering. It also indicated the low adaptive capacity ($C_{ada.}$) needed to maintain the original system performance at a

new performance level after fluctuations. These observations primarily result from low capacity of PV power, the pressure limitations of the pump and low flux (average and cumulative values provided in Table S2, Supporting Information).

It is intuitive that the system should be able to adapt to the fluctuations with the addition of SCs and charge controller; however, this was not achieved at these high salinities due to i) the small rated PV capacity to power the pump and provide the charging current to the SCs (strong power source) simultaneously; ii) the limited energy storage capacity in SCs, indicating the necessity of increasing the energy capacity of the storage units (e.g., more SCs in parallel or batteries). For this reason, in the next section, the PV capacity was varied in a wide range to examine how it affects the ability of SCs and charge controller to reduce system shut-downs and improve system resilience.
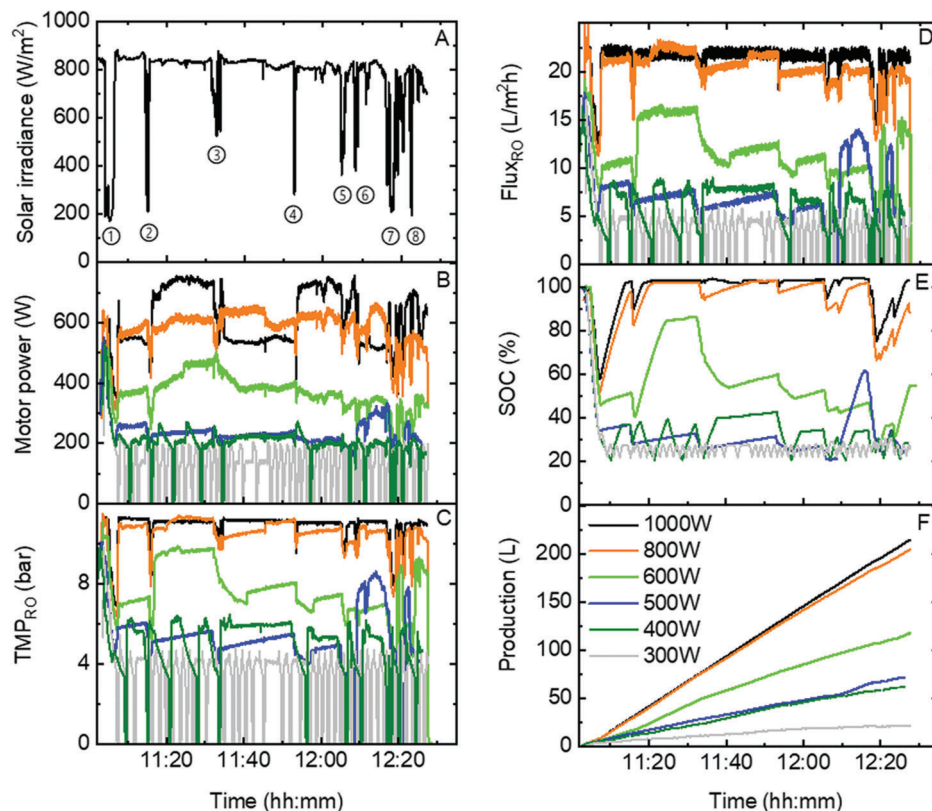
3.4. Impact of PV Power Capacity on System Resilience with SCs Buffering Control

In this section, the aim is to examine how the PV power capacity affects the ability of SCs and charge controller to reduce system shut-downs, as well as improve the resilience to power variations. For the two system configurations, the experiments were conducted at feed salinity of 5.0 g L^{-1} under highly fluctuating conditions on the partly cloudy day by varying the PV power capacity over the range 300, 400, 600, 800 and 1000 W (see **Figure 9**).

For a PV capacity of <500 W, more shut-down events are observed during the fluctuations (Figure 9A)—motor power (Figure 9B) drops to 0 W several times, and along with zero TMP$_{RO}$ and flux (see Figure 9C,D)—due to the inadequate PV power available to charge SCs and drive the pump simultaneously (see Figures S13 and S14, Supporting Information). When a PV power capacity of ≥ 600 W was implemented, no system shut-down occurred (several shut-down events observed on the directly-coupled system, see Figures S10–S12, Supporting Information). High motor power (see Figure 9B, average value >300 W as shown in Table S3, Supporting Information) enabled a high TMP$_{RO}$ to be obtained (Figure 9C) to overcome the osmotic pressure of the feed water (≈ 4 bar) and resulted in large flux (Figure 9D) and daily production (Figure 9F). This reduced the amount of system off-time (hence reduce loading on electronics) and avoids wear on the pump motor by constant restarting, consequently, pump duty point is continuously optimized according to the input power available. Referring to the lowest dips in Figure 9E, the lower limit of SOC exhibited a declining trend (from 55% to 20%) with the decrease of PV power capacity (from 1000 to 300 W). This indicates that SCs are fully discharged due to less power available from PV and maximum power extracted from the pump. A subsequent detailed explanation in terms of the charging/discharging mechanism based on the pre-set voltage sensing thresholds is discussed (current and voltage curves provided in Figure S16 of the Supporting Information).

At the reference PV capacity of 500 W ($I_{mpp} = 2.7$ A, see Table S4, Supporting Information), the V_{PV} recovered back to high voltage in the range of 180–210 V (see Figure S14, Supporting Information) after the SCs were fully discharged at $V_{charging\_off} = 80$ V (SOC = 20%) at dip ⑥ (shut-down in Figure 7). However, I_{PV} only reached ≈ 1.1 A (depending on the SI levels), which was in-

**ADVANCED
SCIENCE NEWS**

www.advancedsciencenews.com

**ADVANCED
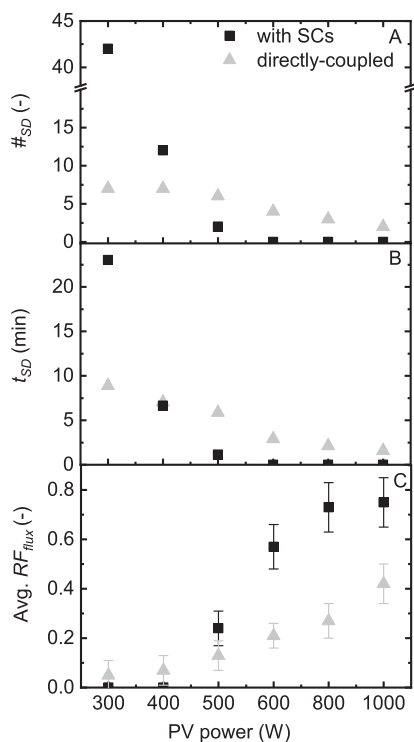SUSTAINABLE
SYSTEMS**

www.advsustainsys.com

Figure 9. Performance of PV-membrane system with SCs and charge controller during the highly variable 90 min period with large SI fluctuations in the middle of the partly cloudy day as a function of PV power capacity (BW30+5.0 g L^{-1} NaCl), illustrating A) solar irradiance, B) motor power, C) TMP$_{RO}$, D) flux$_{RO}$, E) SOC and F) production.

adequate to supply current for operating the pump and charging SCs. The 400 W case (I_{mpp} = 2.1 A, see Table S4, Supporting Information) exhibited higher TMP$_{RO}$ and flux than those in the 500 W case (dark green vs dark blue curves in Figure 9C, D) from dips ①-⑤. This occurred after the system shut-downs and the TMP$_{RO}$ momentarily recovered back to the status of directly-coupled configuration (SCs disconnected) for a short period of time until V_{PV} > $V_{charging\_on}$. The same phenomenon happened when the TMP$_{RO}$ (hence flux) at 500 W exceeded the TMP$_{RO}$ at 400 W once the system was off at dip ⑥. However, more frequent shut-downs in the 400 W case suggested a poorer ability of the charge controller and SCs to reduce the system shut-down events. This has become more evident for the 300 W case with more frequent oscillations being observed (grey curves in Figure 9B–D). When increasing the PV to 600 W, the high I_{PV} (I_{mpp} = 3.2 A) was capable of charging the SCs continuously (with SOC > 30%, see light green curve in Figure 9E) without system shut-downs—a fraction of 3–30% of I_{PV} was used to charge the SCs. Consequently, the SCs can be discharged to the pump (SOC dropping from ≈50 to 30%) when the V_{PV} dropped to 80 V at dip ⑧. Hence, 600 W of PV enabled a better system performance compared with the 500 W case. The benefits of powering with high PV capacity become more apparent on the 800 and 1000 W cases, which can be reflected from i) no shut-down events are observed; ii) the SOC reaching up to 100% when the SI returned to 800 W m^{-2} once more. It is noted that the pump consumed up to 750 W for significant periods of time when the SOC reached ≈100% at PV of 1000 W (see black

curve in Figure 9E). This occurred due to the fact that all the I_{PV} was extracted by the pump (see Figure S14, Supporting Information). The disadvantage is the induced power loss across the lamp (estimated to be ≈400 W, as detailed in Section 2.1) when the SOC reached up to 100%. However, the shut-down events are largely improved. In summary, increased PV power available can significantly reduce the system shut-down events and enhance system resilience. Repeated experiments were carried out to demonstrate repeatable results as provided in Figure S15 of the Supporting Information. Overall, the results showed good repeatability of electrical performance (motor power, variations calculated to be 2.4%) as well as membrane performance (TMP$_{RO}$, flux$_{RO}$, variations calculated to be 3%) at varied PV power capacity, while the small variations were within systematical error (5.4%). These results highlight the repeatable characterization data can be obtained by following the system operation strategy in this PV-membrane system (Section S1 in Supporting Information).

To quantify the above observations in system shut-down events and flux resilience, the #$_{SD}$ and t_{SD}, average RF_{flux} have been investigated as a function of PV power capacity. The averaged results at all different fluctuations (dips ①-⑧ in Figure 2B) are plotted in **Figure 10**.

Referring to Figure 10A,B, the #$_{SD}$ and t_{SD} exhibited a decreasing trend with the increase of PV power capacity regardless of the system configuration. Once adding the SCs and charge controller, the #$_{SD}$ become worse at low PV capacity <500 W, the reasons for this have been discussed above. Overall the dips from

**ADVANCED
SCIENCE NEWS**

www.advancedsciencenews.com

**ADVANCED
SUSTAINABLE
SYSTEMS**

www.advsustainsys.com

Figure 10. Resilience factor as a function of PV power capacity in the PV-membrane system with/without SCs buffering control during the highly variable 90 min period with large SI fluctuations in the middle of the partly cloudy day. A) $\#_{SD}$, B) t_{SD} and C) average RF_{flux}. The error bars were estimated by using error propagation method (see Section S6 of the Supporting Information).

① to ⑧, the averaged RF_{flux} (>0.3, see Figure 10C) was largely increased at PV power ≥500 W, in particular, the values rose to 0.8 when the SCs and charge controller were incorporated. The improvement is due to i) the improved flux after disruption (F_d) due to the SCs buffering at low SI; ii) higher flux after recovery (high F_r); iii) higher initial flux (F_0) due to high driving force from the pump. As a result, the PV-membrane system is more resilient when equipped with a high PV capacity as well as the SCs and charge controller. Overall, these results on $\#_{SD}$, t_{SD}, average RF_{flux} during the severe fluctuations confirmed that the system shut-downs and resilience were improved by increasing the PV power capacity, albeit at increased initial investment cost. With this energy capacity (21 Wh), PV power of 800 W is demonstrated to be a better capacity for both pump operation (no shut-down events) and energy buffering (more resilient system). However, the increased costs are difficult to quantify to derive an overall water cost depending, among other things, on the average SI levels on site and the feed water quality. Moreover, the application of high energy capacity SCs can be used for buffering longer period of fluctuations for the future work in the PV-membrane systems.

4. Conclusions

The potential of SCs energy buffering and charge controller to reduce system shut-down events and enhance system resilience on a PV-membrane system was investigated under varied full-

length solar days (sunny, partly cloudy, and very cloudy days) at 1 s resolution with a duration of 9–12 h. The quantitative assessment of the system resilience—$\#_{SD}$, t_{SD}, cumulative TDS, and average RF_{flux} under 90 min of SI fluctuations—have been carried out with two operation modes i) directly-coupled and ii) with SCs and charge controller.

When the directly-coupled PV-membrane system was operated with a BW30 RO membrane at a feed salinity of 5.0 g L^{-1} NaCl at rated PV capacity of 500 W, the system was more resilient on the partly cloudy and sunny days than on the very cloudy day due to the minimal number of fluctuations. Once adding the SCs and charge controller, the t_{SD} was reduced by 37% (partly cloudy day) and 12% (very cloudy day). Instead, the $\#_{SD}$ was reduced by 2–13 events on these two solar days. The average SEC was improved by 22% (very cloudy day) and 8% (sunny day), with comparable SEC values on partly cloudy day. During the high 90 min fluctuations on the partly cloudy day with the addition of the SCs and charge controller, at varied feed salinity from 1.0 to 10.0 g L^{-1}, it was found that the RF_{flux} increased to ≈0.3 at feed salinity ≤5.0 g L^{-1}, whereas it exhibited the opposite direction at feed salinity of 7.5 and 10.0 g L^{-1}. As a result, the PV-membrane system is more resilient to flux variations with energy buffering up to salinity of 5.0 g L^{-1}, but limited to the high feed salinity (7.5 and 10.0 g L^{-1} NaCl) based on the rated PV capacity of 500 W. When varying the PV power capacity, no system shut-down events were observed at PV power capacity ≥600 W and the RF_{flux} values rose from 0.3 to 0.8, both indicating the system is more resilient to changes in SI, while working with high PV capacity. These findings highlight the ability of the charge controller and SCs buffering to reduce system shut-downs and enhance resilience to deal with the fluctuations encountered over a range of different solar days. For future work, the implementation of pulse width modulation is required to reduce the power loss and eliminate the lamp, the control algorithm based on the ramp rates threshold is recommended to adapt to the fast change of the SI. Meanwhile, high energy storage capacity is recommended to provide a longer period of energy buffering in the PV-membrane system.

Supporting Information

Supporting Information is available from the Wiley Online Library or from the author.

Conflict of Interest

The authors declare no conflict of interest.

2300031 (14 of 16)

Data Availability Statement

The data that support the findings of this study are available from the corresponding author upon reasonable request.

[1] A. Ali, R. A. Tufa, F. Macedonio, E. Curcio, E. Drioli, *Renewable Sustainable Energy Rev.* **2018**, *81*, 1.

[2] F. Calise, F. L. Cappiello, R. Vanoli, M. Vicidomini, *Appl. Energy* **2019**, *253*, 113575.

[3] World Health Organization, *Safely managed drinking water*, https://data.unicef.org/wp-content/uploads/2017/03/safely-managed-drinking-water-JMP-2017-1.pdf (accessed: March 2023).

[4] United Nations, *The Sustainable Development Goals Report 2022*, https://unstats.un.org/sdgs/report/2022/The-Sustainable-Development-Goals-Report-2022.pdf (accessed: March 2023).

[5] Fraunhofer ISE, Photovoltaics report, updated: 21 February 2023, https://www.ise.fraunhofer.de/content/dam/ise/de/documents/publications/studies/Photovoltaics-Report.pdf (accessed: March 2023).

[6] M. K. Shahid, B. Mainali, P. R. Rout, J. W. Lim, M. Aslam, A. E. Al-Rawajfeh, Y. Choi, *Water* **2023**, *15*, 534.

[7] M. C. Garg, in *Current Trends and Future Developments on (Bio-) Membranes* (Eds.: A. Basile, A. Cassano, A. Figoli), Elsevier, Amsterdam **2019**, pp. 85.

[8] D. B. Riffel, P. C. M. Carvalho, *Desalination* **2009**, *247*, 378.

[9] A. M. Bilton, L. C. Kelley, S. Dubowsky, *Desalin. Water Treat.* **2012**, *31*, 24.

[10] A. I. Schäfer, J. Shen, B. S. Richards, *npj Clean Water* **2018**, *1*, 1.

[11] B. O. Kang, K.-S. Tam, *Appl. Energy* **2015**, *137*, 240.

[12] M. F. Roslan, M. A. Hannan, P. J. Ker, M. N. Uddin, *Appl. Energy* **2019**, *240*, 583.

[13] I. Ranaweera, O.-M. Midtgård, G. H. Yordanov, in *29th European Photovoltaic Solar Energy Conf. and Exhibition*, **2014**, pp. 2635–2638.

[14] J. F. Manwell, J. G. McGowan, *Wind Energy Explained: Theory, Design and Application*, 2nd ed., John Wiley & Sons Ltd., New York **2009**.

[15] J. M. Vindel, J. Polo, *Atmos. Res.* **2014**, *143*, 313.

[16] G. L. Park, A. I. Schäfer, B. S. Richards, *Renewable Energy* **2013**, *50*, 126.

[17] M. Freire-Gormaly, A. M. Bilton, *Desalination* **2018**, *435*, 188.

[18] A. Ruiz-García, I. Nuez, *Desalination* **2020**, *489*, 114526.

[19] Y.-A. Boussouga, B. S. Richards, A. I. Schäfer, *J. Membr. Sci.* **2021**, *617*, 118452.

[20] B. S. Richards, D. P. S. Capão, W. G. Früh, A. I. Schäfer, *Sep. Purif. Technol.* **2015**, *156*, 379.

[21] J. Shen, A. Jeihanipour, B. S. Richards, A. I. Schäfer, *Sep. Purif. Technol.* **2019**, *221*, 64.

[22] P. Cabrera, J. A. Carta, J. González, G. Melián, *Desalination* **2018**, *435*, 77.

[23] M. Thomson, D. Infield, *Desalination* **2005**, *183*, 105.

[24] W. Lai, Q. Ma, H. Lu, S. Weng, J. Fan, H. Fang, *Desalination* **2016**, *395*, 17.

[25] H.-P. Ma, H.-L. Wang, Y.-H. Qi, Z.-L. Chao, L. Tian, W. Yuan, L. Dai, W.-J. Lv, *J. Membr. Sci.* **2022**, *644*, 120141.

[26] DuPont water solutions: FilmTec™ reverse osmosis membranes technical manual – Form No. 609-00071-0109, https://www.dupont.com/content/dam/dupont/amer/us/en/water-solutions/public/documents/en/RO-NF-FilmTec-Manual-45-D01504-en.pdf (accessed: March 2023).

[27] M. Freire-Gormaly, A. M. Bilton, *J. Membr. Sci.* **2019**, *583*, 220.

[28] G. L. Park, A. I. Schäfer, B. S. Richards, *Water Sci. Technol.* **2012**, *65*, 867.

[29] G. L. Park, A. I. Schäfer, B. S. Richards, *J. Membr. Sci.* **2011**, *370*, 34.

[30] A. Dutta, J. Mahanta, T. Banerjee, *Adv. Sustainable Syst.* **2020**, *4*, 2000182.

[31] A. R. Dehghani-Sanij, E. Tharumalingam, M. B. Dusseault, R. Fraser, *Renewable Sustainable Energy Rev.* **2019**, *104*, 192.

[32] A. G. Olabi, C. Onumaegbu, T. Wilberforce, M. Ramadan, M. A. Abdelkareem, A. Hai Al - Alami, *Energy* **2020**, *11*, 2696.

[33] T. M. Gür, *Energy Environ. Sci.* **2018**, *11*, 2696.

[34] S. Li, Y.-H. Cai, A. I. Schäfer, B. S. Richards, *Appl. Energy* **2019**, *253*, 113524.

[35] VARTA: VARTA pulse /pulse neo, https://www.varta-storage.com/fileadmin/varta_storage/downloads/products/energy/varta-pulse/Datasheet_VARTA_pulse_en_17.pdf (accessed: May 2022).

[36] P. Donovan, Lithium-ion batteries offer a definitive, sustainable and cost-effective advantage for UPS, https://www.datacenterdynamics.com/opinions/lithium-ionbatteries-offer-definitive-sustainable-and-cost-effective-advantage-ups/ (accessed: November 2020).

[37] B. Diouf, R. Pode, *Renewable Energy* **2015**, *76*, 375.

[38] C.-S. Karavas, K. G. Arvanitis, G. Kyriakarakos, D. D. Piromalis, G. Papadakis, *Sol. Energy* **2018**, *159*, 947.

[39] A. Soric, R. Cesaro, P. Perez, E. Guiol, P. Moulin, *Desalination* **2012**, *301*, 67.

[40] S. Victor, Usage of supercapacitors in wind turbine pitch control systems: Economic analysis, https://www.vinatech.com/winko.php?code=blog_e&v=eng&body=view&page=1&number=52&category=&keyfield=&key=#sub_check (accessed: August 2022).

[41] M. Şahin, F. Blaabjerg, A. Sangwongwanich, *Energies* **2022**, *15*, 674.

[42] P. K. S. Roy, H. Bora Karayaka, J. He, Y.-H. Yu, Economic comparison between a battery and supercapacitor for hourly dispatching wave energy converter power: Preprint. Golden, CO: National Renewable Energy Laboratory. NREL/CP-5000-77398, https://www.nrel.gov/docs/fy21osti/77398.pdf (accessed: August 2022).

[43] S. Li, A. Voigt, A. I. Schäfer, B. S. Richards, *Renewable Energy* **2020**, *149*, 877.

[44] M. T. Mito, X. Ma, H. Albuflasa, P. A. Davies, *Renewable Sustainable Energy Rev.* **2019**, *112*, 669.

[45] E. T. Maddalena, C. G. d. S. Moraes, G. Braganca, L. G. Junior, R. B. Godoy, J. O. P. Pinto, *IEEE Trans. Ind. Appl.* **2019**, *55*, 2263.

[46] A. Schies, J. Went, C. Heidtmann, M. Eisele, F. Kroemke, H. Schmoch, M. Vetter, *Desalin. Water Treat.* **2010**, *21*, 131.

[47] J. A. Carta, J. González, P. Cabrera, V. J. Subiela, *Appl. Energy* **2015**, *137*, 222.

[48] M. T. Mito, X. Ma, H. Albuflasa, P. A. Davies, *Desalination* **2022**, *532*, 115715.

[49] C. C. K. Liu, J. W. Park, R. Migita, G. Qin, *Desalination* **2002**, *150*, 277.

[50] A. A. Kamel, H. Rezk, M. A. Abdelkareem, *Int. J. Hydrogen Energy* **2021**, *46*, 6061.

[51] C.-S. Karavas, E. Dimitriou, A. T. Balafoutis, D. Manolakos, G. Papadakis, *Green Energy Sustainability* **2022**, *2*, 1.

[52] G. Kyriakarakos, A. I. Dounis, K. G. Arvanitis, G. Papadakis, *Appl. Energy* **2017**, *187*, 575.

[53] M. A. Soleimanzade, A. Kumar, M. Sadrzadeh, *Appl. Energy* **2022**, *317*, 119184.

[54] M. A. Soleimanzade, M. Sadrzadeh, *Appl. Energy* **2021**, *293*, 116959.

[55] N. Argaw, D. Colorado, Renewable energy water pumping systems handbook, NREL/SR-500-30481, https://www.nrel.gov/docs/fy04osti/30481.pdf (accessed: May 2022).

[56] EnergyTrend: Price trend: Polysilicon and wafer prices expected to rise continuously as high cost and production restrictions inhibit mid and downstream operating rate relentlessly, https://www.energytrend.com/solar-price.html (accessed: January 2022).

[57] M. A. Alghoul, P. Poovanaesvaran, M. H. Mohammed, A. M. Fadhil, A. F. Muftah, M. M. Alkilani, K. Sopian, *Renewable Energy* **2016**, *93*, 101.

[58] S. I. Bouhadjar, H. Kopp, P. Britsch, S. A. Deowan, J. Hoinkis, J. Bundschuh, *J. Environ. Manage.* **2019**, *231*, 1263.

[59] A. Zein, S. Karaki, M. Al-Hindi, *Renewable Energy* **2023**, *208*, 385.

[60] P. A. Koklas, S. A. Papathanassiou, *Renewable Energy* **2006**, *31*, 2122.

[61] F. Greco, S. G. J. Heijman, A. Jarquin-Laguna, *Processes* **2021**, *9*, 2181.

[62] P. Gasser, P. Lustenberger, M. Cinelli, W. Kim, M. Spada, P. Burgherr, S. Hirschberg, B. Stojadinovic, T. Y. Sun, *Sustainable Resilient Infrastruct.* **2019**, *6*, 273.

[63] S. Li, A. P. S. G. d. Carvalho, A. I. Schäfer, B. S. Richards, *Appl. Sci.* **2021**, *11*, 856.

[64] F. Liu, Y. Kang, Y. Zhang, S. Duan, in *2008 3rd IEEE Conf. on Industrial Electronics and Applications*, IEEE, Piscataway, NJ **2008**, pp. 804.

[65] DuPont water solutions: Inge dizzer P – Ultrafiltration modules, https://www.lenntech.com/Data-sheets/Inge-Dizzer-P-L.pdf (accessed: December 2021).

[66] USGS water availability and use science program: National brackish groundwater assessment, https://www.water.usgs.gov/ogw/gwrp/brackishgw/brackish.html, **2022** (accessed: January 2022).

[67] D. Chen, Y. Wang, M. Hong, *Nano Energy* **2012**, *1*, 73.

[68] A. I. Schäfer, A. Broeckmann, B. S. Richards, *Environ. Sci. Technol.* **2007**, *41*, 998.

[69] B. S. Richards, D. P. S. Capão, A. I. Schäfer, *Environ. Sci. Technol.* **2008**, *42*, 4563.

[70] R. B. McCleskey, D. K. Nordstrom, J. N. Ryan, *Limnol. Oceanogr. Methods* **2012**, *10*, 952.

[71] A. F. Rusydi, *IOP Conf. Ser.: Earth Environ. Sci.* **2018**, *118*, 012019.

[72] Chroma: Programmable DC power supply (62000 H series) operating & programmable manual, http://www.chromausa.com/pdf/62000H%20Datasheet_0123.pdf (accessed: March 2023).

[73] Sunmodule SW 100 poly RGP, https://www.boutiquesolaire.fr/Docs/Solarworld/SW_poly_100-24.pdf (accessed: December 2021).

[74] P. Juan-Garcia, D. Butler, J. Comas, G. Darch, C. Sweetapple, A. Thornton, L. Corominas, *Water Res.* **2017**, *115*, 149.

[75] H. T. Tran, M. Balchanos, J. C. Domerçant, D. N. Mavris, *Reliab. Eng./Syst. Saf* **2017**, *158*, 73.

[76] World Health Organisation: Guidelines for drinking water quality, 4th edition, incorporating the 1st addendum, https://www.who.int/publications/i/item/9789241549950 (accessed: December 2021).

[77] B. S. Richards, G. L. Park, T. Pietzsch, A. I. Schäfer, *J. Membr. Sci.* **2014**, *468*, 224.